# Flexible operation strategy for formic acid synthesis providing frequency containment reserve in smart grids

Arash E. Samani[a,b], Jeroen D. M. De Kooning[a,c], César A. Urbina Blanco[d], Lieven Vandevelde[a,b]

[a] *Department of Electromechanical, Systems and Metal Engineering, Ghent University, Tech Lane Ghent Science Park-Campus Ardoyen, Technologiepark Zwijnaarde 131, B-9052 Ghent, Belgium*
[b] *FlandersMake@UGent - Corelab EEDT-DC*
[c] *FlandersMake@UGent - Corelab EEDT-MP*
[d] *Laboratory for Chemical Technology (LCT), Department of Materials, Textiles and Chemical Engineering, Ghent University, Tech Lane Ghent Science Park-Campus Ardoyen, Technologiepark Zwijnaarde 125, B-9052 Ghent, Belgium*

**Abstract**

The demand-side contribution to grid frequency regulation is becoming increasingly important due to the growing penetration of renewable energy in the power system. Among energy-intensive industrial loads, chemical plants have a high potential to offer grid balancing services due to their existing control infrastructure and storage capabilities. However, applying fast ramp rates and providing time-critical grid services is not straightforward due to strict constraints and the nonlinear dynamics of chemical systems. Therefore, adaptive operating approaches are required to increase the process's flexibility and facilitate the fast demand response operation. This work proposes a flexible operating strategy for the cooperative operation of a Polymer Electrolyte Membrane (PEM) electrolyser and multi-stage compression systems in a chemical process to provide Frequency Containment Reserve (FCR). This strategy aims to realise the desired power regulation dynamics on the grid side while maintaining the reactor's optimal operating conditions, i.e., temperature, pressure and flow rate ratio. A techno-economic analysis is performed to obtain optimal operating points. The techno-economic analysis shows that operating the process at a baseload of 73% while offering the remaining capacity as a power reserve can create additional revenue and improve the economic profit by around 10%. The proposed approach is validated by dynamic simulations of a Carbon Capture and Utilisation (CCU) process for formic acid production. The results show that the proposed strategy can enhance the process's operational flexibility and enable FCR provision with a limited impact on reactor efficiency (<1%).

*Keywords:*
Demand response, Electrical power systems, Frequency containment reserve, Carbon capture and utilization, Formic acid

**Acronyms**

| | |
|---|---|
| AAR | Acid to Amine Ratio |
| aFRR | automated Frequency Restoration Reserve |
| BOP | Balance-Of-Plant |
| BSPs | Balancing Service Providers |
| CCU | Carbon Capture and Utilisation |
| FCR | Frequency Containment Reserve |
| FSPs | Flexibility Service Providers |
| LNG | Liquefied Natural Gas |
| mFRR | manual Frequency Restoration Reserve |
| MPC | Model Predictive Control |
| PEM | Polymer Electrolyte Membrane |
| PI | Proportional Integral |
| PMSM | Permanent Magnet Synchronous Machine |
| RW | Randles-Warburg |
| SCP | Single-Cell Protein |
| TRL | Technology Readiness Level |
| TSO | Transmission System Operator |

**Nomenclature**

| | |
|---|---|
| $\alpha$ | Baseload factor |
| $\beta$ | Minimum capacity factor |
| $\delta f$ | Frequency deviation |
| $\delta P$ | Power reserve |
| $\eta$ | Electrolyser partial load efficiency |
| $\omega$ | Compressor speed |
| $\Psi_c$ | Compressor pressure ratio |
| Obj | Objective function |
| $C_{\mathrm{dl}}$ | Double-layer capacitance |
| $E_0$ | Standard electrode potential |
| $E_{\mathrm{el}}$ | Electricity price |
| $E_{\mathrm{FA}}$ | Formic acid price |
| $E_{\mathrm{FCR}}$ | FCR price |
| $f$ | Grid frequency |
| $H_2^{\mathrm{p}}$ | Electrolyser hydrogen production |
| $I_{\mathrm{in}}$ | PEM electrolyser current |
| $k$ | Droop constant |
| $m_{\mathrm{nom}}$ | Compressor nominal flow rate |
| $m_{\mathrm{op}}$ | Compressor operating flow rate |
| $m_{\mathrm{r}}$ | Compressor relative flow rate |

*Email address:* ebnealisamani.arash@ugent.be (Arash E. Samani)

| | |
|---|---|
| $P_b$ | Baseload power |
| $P_e$ | Operating power |
| $P_{max}$ | Maximum capacity |
| $P_{min}$ | Minimum capacity |
| $P_{nom}$ | Electrolyser nominal power |
| $Q_{FA}$ | Formic acid flow rate |
| $R_{ct}$ | Activation losses |
| $R_m$ | Membrane ohmic losses |
| $R_t$ | Charge transfer resistance |
| $T$ | Period |
| $t$ | Time step |
| $V_a$ | Anode activation voltage |
| $V_c$ | Cathode activation voltage |
| $V_{el}$ | Voltage drop across the PEM stack |
| $V_m$ | Membrane ohmic voltage drop |
| $Z_a$ | Anode impedance |
| $Z_c$ | Cathode impedance |
| $Z_{el}$ | PEM stack equivalent impedance |
| $Z_w$ | Warburg impedance |

## 1. Introduction

The transition towards a low carbon future has led to a higher integration of renewable energy sources into the power system. According to the European Green Deal, in line with the Paris Agreement, the EU aims to increase the share of renewable energy by at least 32% and reduce greenhouse gas emissions by at least 40% (compared to 1990 levels) by 2030 [1]. Although the increased share of renewable energy sources in the energy system mitigates the $CO_2$ emissions, it introduces new challenges to the power system management due to the intermittent, non-dispatchable nature of renewable energy [2, 3]. The higher dependency on renewables reduces the system reliability, i.e., stability and security, and increases the load on fossil-based power plants to balance the supply-demand mismatches [4]. Therefore, a new dynamic equilibrium with a higher degree of flexibility is required to ensure the power grid robustness and accommodate higher levels of renewable power generation.

The electrical demand side can provide flexibility by adjusting the load pattern based on grid requirements. Energy-intensive industrial processes with high specific electricity costs, i.e., electricity costs per gross value added [5], are the prime candidates for demand-side integration. The industrial sector flexibility has been primarily studied for the price-based demand response programs, in which the plant operation is scheduled based on the electricity price variation. The price-based demand response has been applied in different industrial applications such as steel furnaces [6], chlorine production [7], ethylene oxide production [8], air separation units [9, 10], cement plants [11], pulp mills [12], and glass furnaces [13]. Although the price-based demand response indirectly helps the Transmission System Operator (TSO) to maintain the balance between supply and demand, there is an increasing need for fast demand response programs such as frequency regulation. Therefore, a continuous response of the industrial loads is needed on a time scale of tens of seconds to tens of minutes to actively support the power system. In Europe, the TSOs offer a full spectrum of frequency ancillary services, including inertial response, Frequency Containment Reserve (FCR), automated Frequency Restoration Reserve (aFRR), and manual Frequency Restoration Reserve (mFRR). These services can be provided by a major electricity consumer, supplier, or trader known as Balancing Service Providers (BSPs) or Flexibility Service Providers (FSPs).

In [14], it is shown that aluminium smelters, Liquefied Natural Gas (LNG) plants, cement processing plants, and greenhouses could be successfully integrated into the power system by providing aFRR. In [5, 15], the technical potential of energy-intensive industries is studied for mFRR provision in Germany. It is shown that electric arc furnaces, chlor-alkali electrolysis, aluminium electrolysis, and cross-sectional technologies such as mills, pumps and compressors can provide an adequate flexibility margin for demand response. In [16], a decentralised control algorithm is developed and tested to regulate the power input of bitumen tanks based on grid frequency variations. A dynamic load control system is implemented for the even distribution of on/off switch actions amongst all tanks. Therefore, the flexible operation of the bitumen tanks is achieved with a limited impact on the temperature of the tanks. In [17], a strategy for providing ancillary services is suggested by switching on/off units with the capability of discrete power changes, e.g., cement crushers or paper mills. It is shown that continuous power regulation can be achieved by combining on/off switching of cement crushers with an on-site energy storage system. Also, Model Predictive Control (MPC) and optimal scheduling are implemented to follow the command load and minimise the switching actions without disturbing the cement kiln. Though the industry's potential for frequency regulation is investigated in literature, the FCR provision has not been taken forward in most industrial loads due to the time-critical requirement of this service and the operational complexities, i.e., process constraints, ramp rate, safety and efficiency losses. Therefore, further research needs to be carried out to enable the industrial loads to offer FCR.

In the chemical industry, demand response can be provided by exploiting energy systems with a fast dynamic response, i.e., compressors, pumps, fans, electric heaters. In this context, electrolysis processes have been identified early on as potential balancing service providers due to their large electricity consumption and fast dynamics [5, 15]. The flexible operation of a membrane electrolyser in chlor-alkali processes has been investigated in literature [18, 19] for FCR provision. Several chlor-alkali and aluminium smelter plants have already been integrated into the grid through providing fast demand response [20]. In recent years, Polymer Electrolyte Membrane (PEM) electrolysis have received extensive attention to providing ancillary services for the power grid due to their high electricity consumption, flexibility and reactivity [21, 22, 23]. Moreover, PEM electrolyser is an enabling technology for $CO_2$ hydrogenation and can play a key role for direct conversion of $CO_2$ value-added chemicals.

In the transition towards a circular economy, novel chemical

processes are being developed for the direct conversion of $CO_2$ to value-added chemicals, such as formic acid, methanol, and methane. Among these processes, formic acid is one of the most promising routes for $CO_2$ utilisation with widespread applications [24]. Formic acid is a basic chemical that finds use in a variety of applications such as leather and rubber production, textiles, pharmaceuticals, preservatives and antibacterial agents in livestock feed. It can also be used as a building block for the bio-catalytic production of value-added chemicals such as Single-Cell Protein (SCP) to support livestock production. Moreover, formic acid can be used as a hydrogen carrier (53 g $H_2$/L) [25, 26] and as fuel for fuel cells, and it is much less expensive to store than hydrogen. The global production of formic acid has increased from 390 kton/year in 1995 to 762 kton/year in 2019 with a firm growth rate of over 3.8% from 2014 to 2019, mainly produced by hydrolysis of methyl formate [27, 28]. The total trade value of formic acid in 2019 was 290 million US$ [29]. The formic acid market is expected to grow in the near future due to health and environmental concerns, e.g., the ban on using antibiotics in animal feed and silage preservation, and emerging applications, e.g., formic acid fuel cells and hydrogen-based storage systems [28, 30]. According to [24], the direct synthesis of formic acid from $CO_2$ has a Technology Readiness Level (TRL) of 3-5. However, several processes have been patented, and some of them were tested on a pilot scale by BASF and Reactwel for the continuous hydrogenation of $CO_2$ to pure formic acid [27].

These processes, which are referred to as Carbon dioxide Capture and Utilisation (CCU), can utilise the PEM electrolyser flexibility and provide ancillary services for the grid. In this context, the approaches that facilitate the integration of CCU based processes into the power system can tackle two problems at the same time. Firstly, utilising the CCU based processes will reduce carbon dioxide emissions. Secondly, the chemical process as an ancillary service provider can support the power grid, which leads to the further integration of renewable energy sources into the power system. Given these advantages, the chemical industry can play a key role in accelerating a low carbon future transition.

Active participation of large electricity consumers in the FCR market is crucial to maintain the power balance in the future grid with a high integration of renewable energy sources. Although several energy-intensive industries already have the potential capacity to provide frequency regulation services, the following challenges should be addressed to ensure the secure and cost-efficient provision of fast-paced ancillary services:

- Chemical processes have difficulty operating flexibly as BSPs or FSPs since they are planned to run continuously at their nominal capacities with predetermined setpoints.
- Applying fast ramp rates, i.e., the rate of change in power demand, is not straightforward due to their nonlinear dynamics and operational constraints, e.g., safety, product quality and wear.
- The lack of an adaptive control architecture for the flexible operation in chemical processes makes it challenging to satisfy grid services requirements while maintaining process efficiency.
- The economic profit of chemical plants is questioned under flexible operation dealing with grid and market uncertainties.

Motivated by the above, this article investigates the feasibility of providing grid balancing with FCR while capturing $CO_2$ with a thermo-catalytic formic acid synthesis process. An operating strategy is proposed for flexible operation of the process by dynamically regulating process components. For the methodology followed in this research, firstly, the dynamic model of the process elements is developed. The compression stages are modelled in Aspen HYSYS, and simulation results are used to make an integrated model in Matlab/Simulink, including the PEM electrolyser, compressors and the reactor. Then, a control algorithm is designed to operate the electrolyser and compressors flexibly to provide ancillary services while maintaining the desired reactor pressure and temperature, resulting in an optimal efficiency and supporting the downstream processes. Finally, an industry scale formic acid process is used to validate the methodology under these dynamic conditions.

The key contribution is the proposed operating strategy to increase the process's operational flexibility and facilitate the integration of chemical processes into the electrical grid, addressing the main challenges of chemical plants for FCR provision. The main deltas of this research with respect to the state of the art are:

- FCR is provided while ensuring the continuous operation of the process without using additional equipment (e.g. additional storage devices).
- Applying fast ramp rates are enabled by exploiting elements with fast dynamics and implementing a control algorithm based on the cooperative operation of its components, i.e., PEM electrolyser and multi-stage compression units.
- Critical values of the process, i.e., pressure and temperature limits and reaction efficiency, are respected by maintaining the optimal operating condition at the reactor.
- The optimal contribution of the process in the European ancillary market is obtained, which generates additional revenue and improves the economic profit.

The methodology applied in this research is also applicable to different CCU based processes for direct conversion of $CO_2$ to chemical synthesis such as methane or methanol where $CO_2$ and hydrogen are used as raw materials, and the reaction takes place under high pressure. Therefore, the proposed techno-economic model and control architecture offers useful and incentive information for chemical industries to provide grid balancing services and improve the economic viability of CCU based processes.

The remainder of the article is structured as follows: The dynamic model of the CCU based process for formic acid production is described in section 2. The proposed control algorithm for providing FCR is presented in section 3. The techno-economic performance is assessed in section 4. The effectiveness of the control performance is examined in section 5. Finally, the outcomes of the proposed approach are summarised in section 6.

## 2. Process model for formic acid synthesis

A dynamic model is developed for a CCU based process for formic acid production via thermo-catalysis through heterogenisation of ruthenium catalysts, as described in [31]. The model objectives are to simulate the process dynamics under flexible operation and to control the operating condition at the reaction stage. Fig. 1 shows the process flow diagram for conversion of $CO_2$ and $H_2$ to formic acid based on the process developed in [31]. The process consists of five stages: (I) the compression stage, (II) the reaction stage, (III) the formic acid enrichment stage, (IV) the amine exchange stage and (V) the formic acid formation and purification. The process is upscaled to produce 1100 kg/h (10 kt/yr) formic acid using 2464 kg/h of $CO_2$ and 112 kg/h of $H_2$. In the first stage, $CO_2$ and $H_2$ are compressed to reach the required pressure level for the reaction. In the second stage, $CO_2$ is hydrogenated in the presence of a base, triethylamine ($Et_3N$). The function of the base during the hydrogenation is to drive the severely thermodynamically limited equilibrium of $CO_2$ hydrogenation to formic acid ($\Delta G_1 = 22$ kJ.mol$^{-1}$) (1) via the formation of a stable adduct with formic acid ($\Delta G_2 = -19$ kJ.mol$^{-1}$), $Et_3NH^+$:$HCOO^-$ [32, 33]:

$$CO_2(g) + H_2(g) \rightarrow HCOOH(aq) \quad (1)$$

$$CO_2(g) + H_2(g) + Et_3N(aq) \rightleftharpoons Et_3NH^+{:}HCOO^-(aq) \quad (2)$$

In the next stage, water and excess triethylamine are removed from the liquid stream from the catalytic reactor to afford the $Et_3NH^+$:$HCOO^-$ adduct at an Acid to Amine Ratio (AAR) of 2.3 to allow the amine exchange in the next stage. Direct separation of the $Et_3NH^+$:$HCOO^-$ adduct into formic acid and triethylamine is not possible. However, the n-butyl imidazole (*n*BIM) adduct, *n*BIMH$^+$:$HCOO^-$, readily decomposes by heat into formic acid and *n*BIM [34]. Thus, the concentrated $Et_3NH^+$:$HCOO^-$ is combined with n-butyl imidazole (*n*BIM) to form *n*BIMH$^+$ : $HCOO^-$. Then, it is fed into a separation

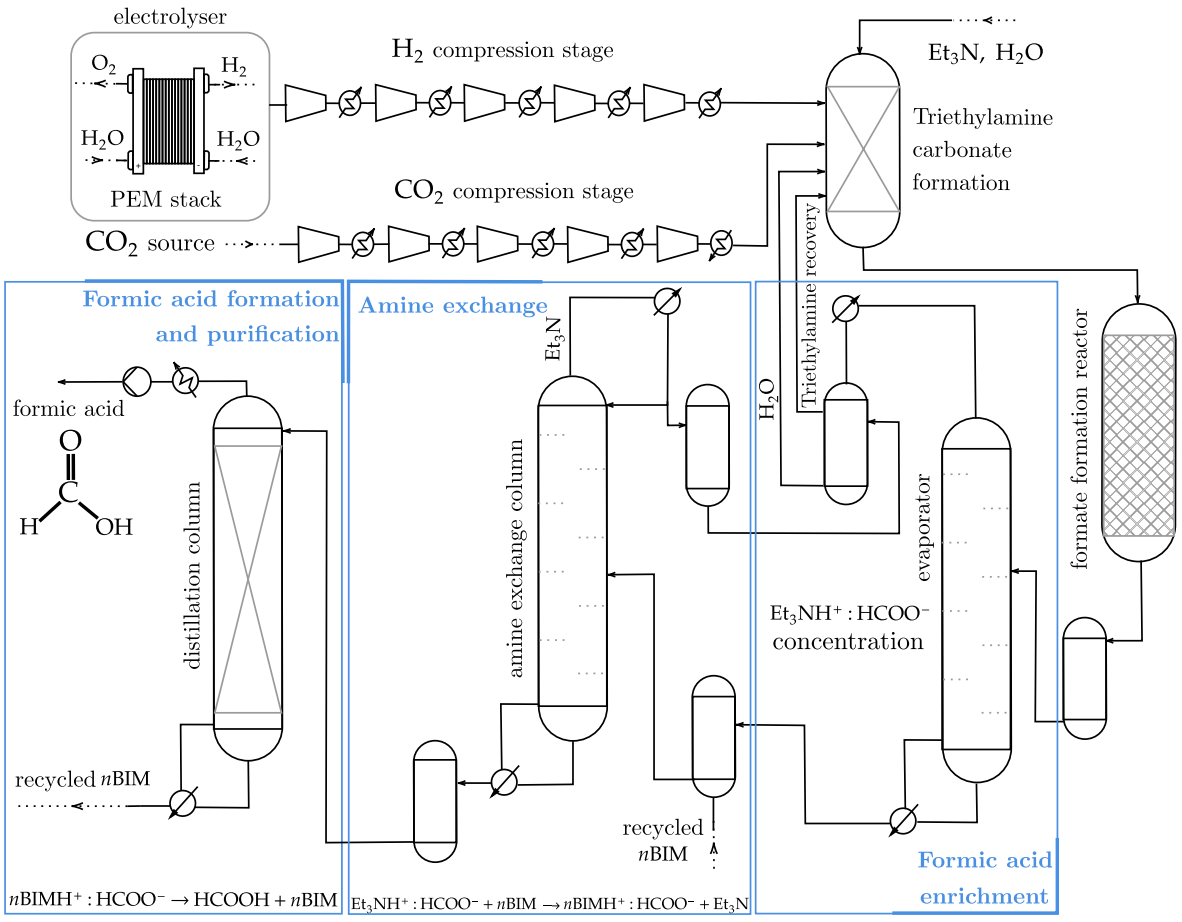


Figure 1: Process flow diagram of formic acid synthesis from $CO_2$ and $H_2$ from PEM electrolyser.

column from which pure formic acid can be obtained as the overhead product according to reactions (3) and (4):

$$Et_3NH^+{:}HCOO^-(l) + n\text{BIM}(l) \rightleftharpoons n\text{BIMH}^+{:}HCOO^-(l) + Et_3N(l) \quad (3)$$

$$n\text{BIMH}^+{:}HCOO^-(l) \rightarrow HCOOH(l) + n\text{BIM}(l) \quad (4)$$

This article focuses on the flexible operation of the process components with fast dynamics, i.e., the PEM electrolyser and compressors, and the impact of this flexible operation on the reaction stage. Though the separation and purification stages are important to produce formic acid, their dynamic behaviour is not included in the simulations. These stages do not interrupt the dynamic response of the electrolyser and compressors, and their slow dynamics dampen the fast variations. However, the parameters such as AAR, reactor productivity, and $CO_2$ conversion are included in the reactor model. Therefore, the reactor output data under the flexible operation can be used to assess the influence on the subsequent process stages. Therefore, the main focus remains on the first three stages of the process, and performance analysis of separation and purification stages are out of scope for this study.

The process is comprised of two main input streams, i.e., $CO_2$ and $H_2$, which are pressurised before feeding into the reactor. The purity of the $CO_2$ source depends on the availability of the captured $CO_2$, and it may come from different sources, i.e., atmosphere, power plant combustion exhaust gasses or waste streams of other processes. This model assumes that the captured $CO_2$ is available at atmospheric pressure and ambient temperature. Therefore, a compression stage is modelled to increase the pressure up to the optimal operating pressure for $CO_2$ hydrogenation. On condition that $CO_2$ is compressed in the upstream process, and it is available at the desired pressure, the compression stage in the preceding process is considered for flexible operation. The compression stage with intermediate cooling stages is modelled in Aspen HYSYS. The $CO_2$ stream is cooled down to 25 °C through intermediate cooling stages to maintain a semi-isothermal compression of compressors, resulting in a high compression efficiency. Based on the simulation results, a five-stage compression system is required to reach the pressure of 120 bar at the reactor. A pressure drop of 0.1 bar is assumed at each intermediate cooling stage. After the compression stage, the $CO_2$ stream is heated to reach 120 °C at the reactor inlet. A 5.79 MW PEM electrolyser generates the required $H_2$ of the process. The $H_2$ stream is compressed through a five-stage compression system up to 120 bar with intermediate cooling stages. The compressors of both stages are assumed to operate at an isentropic efficiency of 80%, which leads to the nominal power of 288 kW and 252 kW for $H_2$ and $CO_2$ compression, respectively.

All process components are separately modelled and integrated into one complete process model in Matlab/Simulink. Fig. 2 illustrates the configuration and connections of electrolyser, Permanent Magnet Synchronous Machine (PMSM) and compressors. The electrochemical model of the PEM stack is developed to represent the impedance behaviour of the PEM electrolyser. The compression stages are first modelled in Aspen HYSYS to identify the specifications, e.g., number of stages and power consumption. Then, each compressor model is built in Simulink and coupled with a PMSM-model to allow variable speed operation. Next, the PEM stack model is connected to the compression stage, taking the hydrogen mass flow rate, pressure and temperature as input signals.

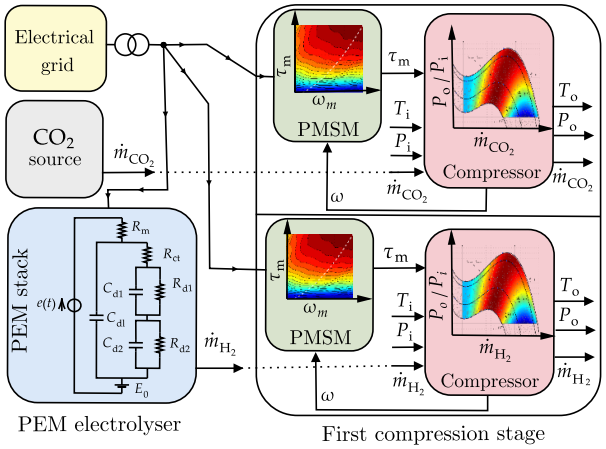


Figure 2: Subsystems configuration and connections: electrolyser, compressor and electrical motor.

### 2.1. PEM Electrolyser

The PEM electrolyser is one of the most energy-intensive components in the process of formic acid synthesis. Also, it has adequate flexibility and agility to regulate its power. The response time from pressurised standby to a full-load operating condition is less than three seconds, and it is below one second for a hot-start. These properties make the PEM electrolyser a prime candidate for engaging in fast-paced ancillary services, e.g., FCR. According to [35, 36, 23] electrolysers can effectively respond to the grid frequency variations, as they are able to respond faster to frequency deviations than gas-turbine and steam-turbine driven synchronous generators. Different applications of PEM electrolysers operating as BSPs or FSPs are investigated in [21, 22]. In [23], it is found that the PEM stack mainly dictates reactivity, and to a lesser degree, Balance-Of-Plant (BOP). Therefore, the PEM stack is modelled to represent the electrolyser dynamics in the formic acid process.

As shown in Fig. 3(a), the electrochemical model of the PEM stack can be described by Randles equivalent circuits connected in series. In the Randles model, electric components represent the dynamic behaviour of different layers in the PEM stack. The voltage drop across the PEM stack $V_{el}$ can be calculated as the difference between the standard electrode potential $E_0$ and the voltage losses including the anode activation voltage $V_a$, cathode activation voltage $V_c$ and the ohmic voltage drop of the membrane $V_m$ [37, 38]:

$$V_{el} = E_0 - V_a - V_c - V_m \quad (5)$$

The equivalent impedance of a PEM stack can be calculated by measuring the current through the PEM stack $I_{in}$ and the voltage across the PEM stack $V_{el}$, which is the sum of the cathode impedance $Z_c$, anode impedance $Z_a$ and the membrane ohmic losses $R_m$:

$$Z_{el} = \frac{V_{el}}{I_{in}} = Z_a + R_m + Z_c \tag{6}$$

As shown in Fig. 3(a), the impedance of each electrode is reflected by the double-layer capacitance $C_{dl}$, the charge transfer resistance $R_t$, and the Warburg impedance of the electrode $Z_w$, ($C_{dl} \parallel [R_t + Z_w]$). The electrical model can be simplified to the Randles-Warburg (RW) model by neglecting the small cathode activation voltage and representing the double layer capacity with a pure, single-frequency theoretical capacity [38, 39]. Fig. 3(b) illustrates the PEM stack electrochemical model using the RW cell. The RW equivalent circuit can be used to model the impedance response of electrochemical systems such as a galvanic cell or an electrolytic cell [40]. The RW values identified in [41] are upscaled to achieve the desired impedance behaviour of the 5.79 MW PEM electrolyser. Table 1 gives the values of these parameters.

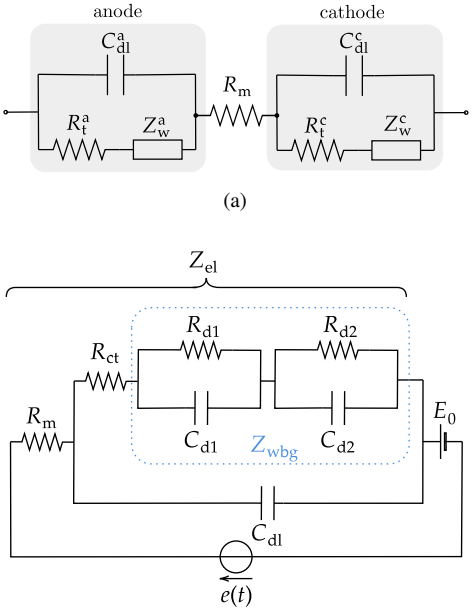


Figure 3: (a) Electrical model of the PEM stack (b) PEM stack electrochemical model with Randles-Warburg cell.

Table 1: Randles-Warburg model parameters.

| $R_{ct}$ (mΩ) | $C_{dl}$ (F) | $R_{d1}$ (mΩ) | $C_{d1}$ (F) | $R_m$ (mΩ) | $R_{d2}$ (mΩ) | $C_{d2}$ (F) |
|---|---|---|---|---|---|---|
| 31.8 | 0.09 | 1.3 | 1.96 | 27.2 | 12.1 | 26.18 |

Fig. 4 shows the dynamic behaviour of the PEM stack model with an ideal current source by means of step responses. The

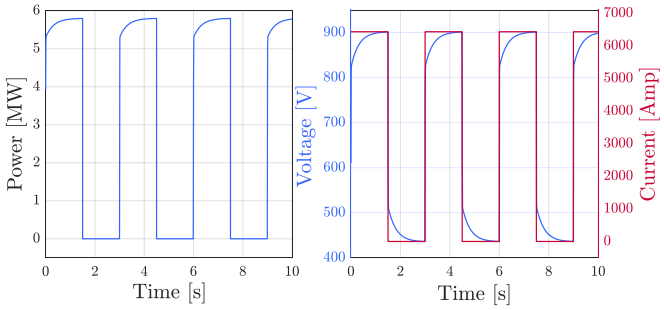


Figure 4: The dynamic response of the PEM stack to the ideal current source.

PEM model reacts to the current changes, and the power signal settles down within one second at maximum, while the PEM voltage reaches 900 V at the rated power. The produced hydrogen $H_2^p$ (kg/h) in function of the operating power $P_e$ (MW) is calculated by (7), considering the partial load efficiency of the electrolyser $\eta = {}^{P_e}/_{P_{nom}}$ [22, 21].

$$H_2^p = \left(-5.9 \cdot \eta^2 + 5.07 \cdot \eta + 20.17\right) \cdot P_e \tag{7}$$

### 2.2. *Compression system*

Two compression stages are modelled for the process of formic acid synthesis to reach the desired pressure level at the reaction stage. The process feed streams, i.e., $H_2$ and $CO_2$, are pressurised up to 120 bar through multi-stage compression systems. The compression stages consist of five centrifugal compressors with intermediate coolers. The multiple-stage compressor trains are first modelled in Aspen HYSYS. The simulation results are used to build up an integrated model including the electrical motors in Simulink.

Under the flexible operating strategy, the process operating condition changes according to the grid frequency variation. Accordingly, the compressors' operating point needs to be adaptively controlled to adjust their operating point based on process requirements. A variable speed motor control can be used to regulate the operating point of the compressors in an energy-efficient manner. Therefore, each compressor is coupled with a PMSM model to enable the compressors to be operated at different rotational speeds. The dynamic model of the PMSMs is developed in the rotating $d$–$q$ synchronous reference frame, taking into account the armature reaction effect, copper losses and iron losses [42]. The compressor model includes the compressor's mechanical dynamics by means of a first order equation of motion including rotational inertia and the compressor and motor torques. The variable-speed control is performed by regulating the motor torque by using field-oriented control [43]. The proposed approach is simulated on each PMSM coupled with a compressor model using an approximation of the compressor performance map.

Fig. 5 shows the compressor data, including the polynomial approximations for four rotational speeds, i.e., 57%, 67%, 95% and 100% of the nominal speed (solid black lines). In order to simulate the performance of the compression systems, the

performance map of the compressors is generated based on the centrifugal compressor data available in Aspen HYSYS. A third-order polynomial approximation of the speed curves is calculated based on the available operating points at each compressor speed. The polynomial of each speed curve can be approximated as:

$$\Psi_c(m_r, \omega) = c_3(\omega)\, m_r^3 + c_2(\omega)\, m_r^2 + c_1(\omega)\, m_r + c_0(\omega) \quad (8)$$

where $\Psi_c$ is the pressure ratio, $\omega$ is the compressor speed, and $m_r$ is the relative flow rate which is the ratio of the operating flow rate $m_{op}$ and the nominal flow rate $m_{nom}$ ($m_r = {}^{m_{op}}/_{m_{nom}}$). In order to simulate the system response accurately, a continuous map of the compressors is required. As the variation of the polynomial coefficients with the rotational speed is approximately linear, the speed curves are interpolated linearly. The third-order polynomial approximations of the speed curves are illustrated with dotted lines in Fig. 5. Moreover, the speed curves are approximated in the efficiency map, and the curves are interpolated by using shape-preserving piecewise cubic interpolation to obtain a continuous compressor efficiency map. Fig. 5 illustrates the efficiency of the compressor as a function of the relative flow rate and the pressure ratio at different rotational speeds.

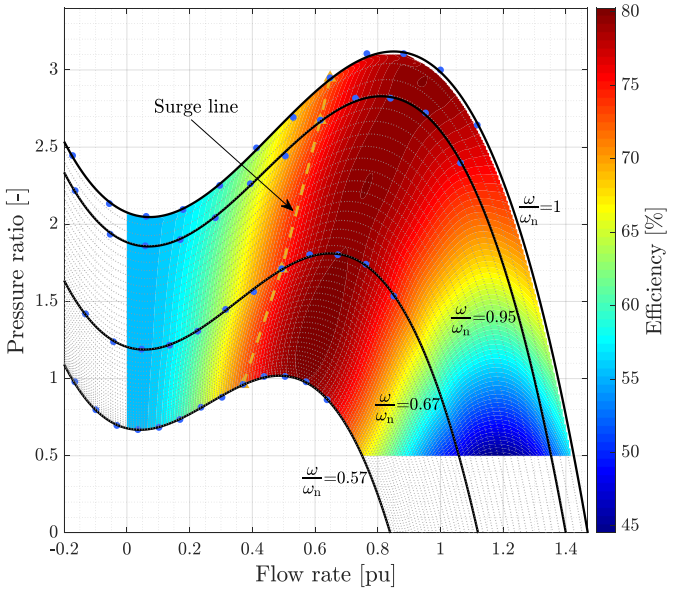


Figure 5: The approximated compressor map: speed curves approximated based on data points (solid lines) and interpolated speed curves (dotted lines).

## 3. Control design

A flexible control approach is required in order to facilitate the integration of the CCU based process into the power grid. The control system must enable the process flexibility at the operational level to satisfy the grid code requirements. The process components with a high degree of flexibility, e.g., the electrolyser, compressors and pumps, can be operated flexibly while respecting the critical values and safety of the process. Therefore, a control algorithm is designed to fulfil two main objectives:

- Providing ancillary services for the grid in the form of frequency containment reserve.
- Maintaining the required operating conditions for the reaction to ensure the desired process efficiency and product quality.

Fig. 6 illustrates the proposed control scheme of the process. The control system of the formic acid synthesis process consists of two main control loops. The primary control loop reacts to the grid frequency variation by regulating the PEM electrolyser power consumption. The second control loop follows the primary controller and regulates the compressor speeds to maintain the optimal level of pressure, temperature and flow rate at the reactor. The different control levels are explained in the following subsections.

### 3.1. PEM electrolyser control: frequency regulation

In the primary control loop, the PEM electrolyser is regulated to follow the grid frequency. Therefore, when the grid frequency deviates from the nominal value, the controller tracks the frequency deviation and adjusts the electrolyser operating point based on a predefined droop. When the frequency falls below the nominal value, i.e., when there is a shortage of power, the electrolyser's power input is reduced to decrease the load on the grid. Conversely, when the frequency is higher than the nominal value, i.e., there is an excess of power, the power setpoint is increased.

The frequency regulation in this work focusses on the standard 200mHz FCR product on the European ancillary service market [44]. Fig. 7 shows the power-frequency chart of the symmetric 200mHz product. In order to provide a symmetrical 200mHz product, the electrolyser reacts to grid frequency deviations within the range of 48.8 to 50.2 Hz. Therefore, the power reserve is fully activated once the frequency deviation reaches 200 mHz. As the FCR product is symmetric, the frequency is stabilised equally for both upward and downward deviations. According to European TSOs' regulations, a deadband of 10 mHz (50 Hz±10 mHz) is considered [45]. In the deadband, the primary control is not allowed to react to the frequency variations, and the electrolyser operates at the baseload power. Therefore, the power setpoint of the electrolyser is calculated as:

$$P_e = \begin{cases} \alpha P_{max} & -0.01 \text{ Hz} \le \delta f \le 0.01 \text{ Hz} \\ \alpha P_{max} + k\delta f & \text{otherwise} \end{cases} \quad (9)$$

where $\alpha$ is the baseload factor as a percentage of the maximum capacity $P_{max}$. The frequency of the grid is represented by $f$. The parameter $\delta f$ is the frequency deviation from 50 Hz ($\delta f = f$ - 50 Hz). The droop constant $k$ is the power-frequency characteristic of the electrolyser calculated based

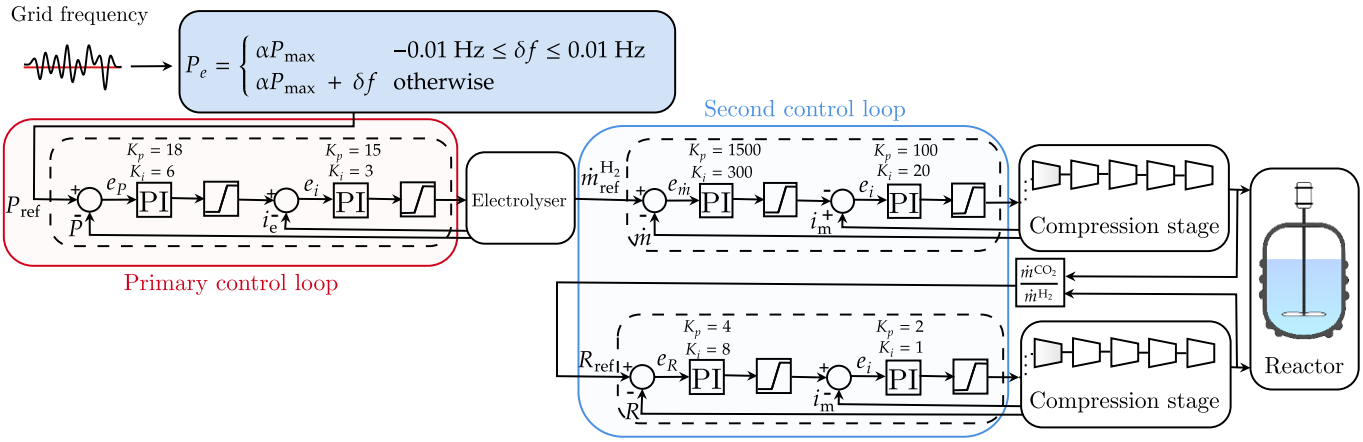


Figure 6: Control system for the flexible operation of process of the formic acid synthesis process based on $CO_2$ and $H_2$.

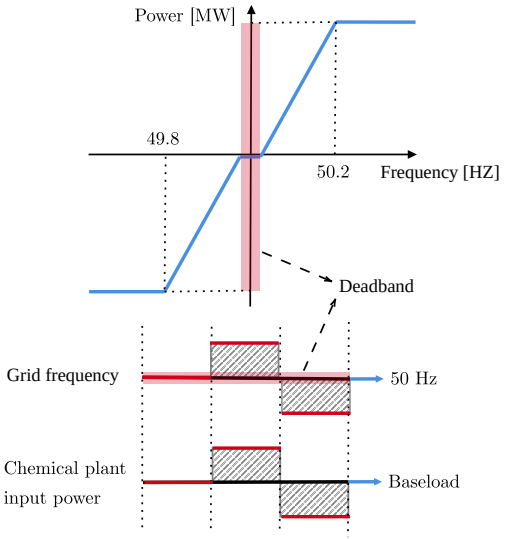


Figure 7: Power-Frequency chart for the symmetric 200mHz FCR product and chemical process operation based on the grid frequency.

on the contractual power reserve $\delta P_{\text{FCR}}$ and the maximum frequency deviation allowed for the FCR product, i.e., 200 mHz, defined as:

$$k = \frac{\delta P_{\text{FCR}}}{\delta f} \tag{10}$$

As illustrated in Fig. 6, a cascaded control system is designed to track the setpoint signal calculated by (9). In the control scheme, the Proportional Integral (PI) controller (outer loop controller) reacts to the grid frequency variation and provides the reference signal to the PEM stack current controller (inner loop controller). Therefore, the cascaded control strategy adjusts the electrolyser power consumption by regulating the PEM stack current.

### 3.2. *Compression stages control system*

As described in the previous section, the primary control modifies the electrolyser power consumption to provide FCR. Therefore, the flow rate of the generated hydrogen at the process input changes based on the grid frequency variation. In this condition, if the compressors are not controlled adaptively and ignore the $H_2$ variation, the optimal operating condition of the reactor will be violated. In the worst case, the pressure and temperature exceed the allowed operating range. In the $H_2$ stream, the compressors' power must be regulated according to the hydrogen generated by the PEM electrolyser. Moreover, the $CO_2$ flow rate needs to be adjusted based on the hydrogen variation to ensure the desired ratio of $H_2$ and $CO_2$ at the reaction stage. Also, the compressors must be controlled to maintain the discharge pressure and temperature at the desired level despite the flow rate variation. Therefore, additional controllers are required to maintain the optimal operating condition of the process. A control system is designed for the $H_2$ and $CO_2$ compression stages to control each compressor's power through variable-speed control. In this control approach, the compressors operate at different rotational speeds by regulating the PMSM torque, using field-oriented control. For instance, if the $H_2$ flow rate reduces, the pressure ratio across the compressor does not change, enabling the compressor to supply a lower flow rate at a reduced speed.

In the $H_2$ compression stage, the first compressor is controlled to track the generated hydrogen and supply the desired pressure at a modified speed. As shown in Fig. 6, in the cascaded control system, the outer PI control loop reacts to the generated hydrogen and sends the reference signal to the inner loop PI controller, which controls the rotational speed by regulating the motor torque. If the following four compressors in the compression stage operate at their maximum power, their discharge pressure and temperature will change with the flow rate variation, which negatively impacts reaction efficiency. Therefore, the other four compressors are controlled to adjust their rotational speed based on the flow rate dictated by the first compressor. As illustrated in Fig. 8, the reference

speed signal is generated by a lookup table obtained from the characteristic curve of each compressor (Fig. 5), and the speed signal is tracked by regulating the motor torque. Therefore, each compressor pressure's ratio remains at the designed value, allowing the compressors to supply the variable flow rate at the modified speed.

The first compressor in the $CO_2$ compression stage is controlled to track the generated hydrogen and regulate the $CO_2$ flow rate to maintain the $CO_2$ and $H_2$ ratio at the optimal level. As shown in Fig. 6, in the cascaded control system, the outer PI controller reacts to the $H_2$ and $CO_2$ ratio and sends the reference signal to the motor torque controller (inner controller). Therefore, the cascaded control regulates the $CO_2$ flow rate by controlling the compressor speed. The following compressors in the compression stage modify their rotational speed based on the flow rate dictated by the first compressor.

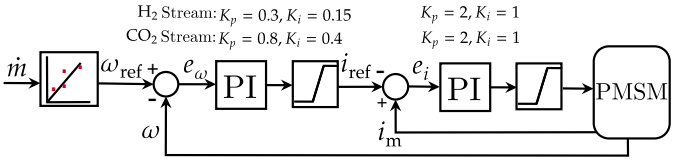


Figure 8: The control diagram for regulating the speed of the last four compressors in the compression stages.

## 4. Techno-economic analysis

Before studying the performance of the proposed control structure, the optimal range of the power reserve and the baseload setpoint need to be determined. Therefore, in this section, a techno-economic analysis is formulated based on market prices, formic acid production and FCR provision.

An industrial-scale $CO_2$-based formic acid process is energy-intensive. In [46], it is shown that reducing the electricity cost is a driving factor to improve the economic performance of the process. Also, it is shown that hydrogen production consumes around 90% of the total electricity consumption through electrolysis, which is 40% of the required energy for the whole process. In [21, 22], it is discussed that participating in the ancillary markets can improve the economic efficiency of hydrogen production. Therefore, offering ancillary services for the grid can generate additional revenues, reducing the formic acid production cost to become competitive with conventional methods.

In order to compare the economic performance of flexible operation with the full-load operation, the profit estimation of the process is formulated by considering the main parameters that vary by the flexible operation, i.e., electricity cost, formic acid production and ancillary service revenue. It is assumed that other cost function parameters, which are slightly disrupted by flexible operation, remain unchanged. Therefore the objective function is defined as:

$$\text{Obj} = \max \sum_{t=1}^{T} (Q_{\text{FA}}(t) \cdot E_{\text{FA}}) - \sum_{t=1}^{T} (P_{\text{e}}(t) \cdot E_{\text{el}}) + \delta P_{\text{FCR}} \cdot E_{\text{FCR}} \cdot T \tag{11}$$

The objective function is evaluated over a period $T$ of one year with a time stepping $t$ of 10 s. The first term represents the income from the formic acid production. It is the sum of the formic acid flow rate $Q_{\text{FA}}$ in kg/h, which varies by regulating the electrolysers operating point, multiplied by the value of formic acid $E_{\text{FA}}$, which is a fixed value. The second term is the electricity cost, which is the power consumed $P_{\text{e}}$ multiplied by the electricity price $E_{\text{el}}$. The operating power $P_e$ is calculated by $P_e = P_b + k\delta f$, where the baseload power $P_b = \alpha P_{\text{max}}$ is a setpoint for the control system responding to the frequency variation. The third term is the revenue from the provision of FCR, which is a product of the reserved power $P_{\text{FCR}}$, the FCR price $E_{\text{FCR}}$ and time $T$. The revenue from FCR is not based on the actual power $P_{\text{e}}$, but only on the contracted reserve $P_{\text{FCR}}$, i.e., it is a standby remuneration, not an activation remuneration. The actual power $P_{\text{e}}$ continuously follows the grid frequency $f$ variations. The power $P_{\text{e}}$ is calculated using (9). $Q_{\text{FA}}$ is calculated by a quadratic function for hydrogen production between 2.3 and 112.0 kg/h:

$$Q_{\text{FA}}(t) = -0.06 \cdot H_2^{\text{p}}(t)^2 + 19.42 \cdot H_2^{\text{p}}(t) - 40.44 \tag{12}$$

where $H_2^{\text{p}}$ can be calculated by using (7).

The objective function (11) is subjected to the following constraints:

$$P_{\text{b}} + \delta P_{\text{FCR}} \leq P_{\text{max}} \tag{13}$$

$$-P_{\text{b}} + \delta P_{\text{FCR}} \leq -P_{\text{min}} \tag{14}$$

and the following bounds:

$$P_{\text{min}} \leq P_{\text{b}} \leq P_{\text{max}}$$

$$0 \leq \delta P_{\text{FCR}} \leq \frac{1}{2}(P_{\text{max}} - P_{\text{min}})$$

where the minimum capacity $P_{\text{min}}$ of 10% is considered to ensure the continuous operation of the electrolyser. This avoids the start-up and shut-down time required to purge the nitrogen. Therefore, the baseload power is limited between minimum capacity $P_{\text{max}}$ and the maximum capacity $P_{\text{max}}$ (0.58 MW to 5.8 MW). In order to provide a symmetrical 200 mHz FCR product and keep the power reserve available for both a positive and a negative variation of the grid frequency, the power reserve $\delta P_{\text{FCR}}$ is defined to not exceed half of the available capacity $(P_{\text{max}} - P_{\text{min}})$. The power reserve and the market prices are assumed to be constant for the whole year. The FCR price is equal to the average price of the 200mHz FCR product in 2021 (January-August), i.e., 19.6 €/MW/h. The electricity price in the model is equal to the average electricity price in Epex Spot in 2021 (January-August), i.e., 62.2 €/MWh. The formic acid price is considered 0.5 €/kg [46].

The objective function (11) finds the optimum operating point in which the profit function is maximised. Fig. 9 shows the profit as a function of baseload. Also, the formic acid production, hydrogen and $CO_2$ consumption are presented at

different baseloads. As it can be seen, offering FCR and operating the electrolyser with a baseload of 73% maximises the profit function, which results in the profit improvement of around 10% compared to the full-load operation. Nevertheless, the flexible operation at the optimum baseload reduces the formic acid production by 13%.

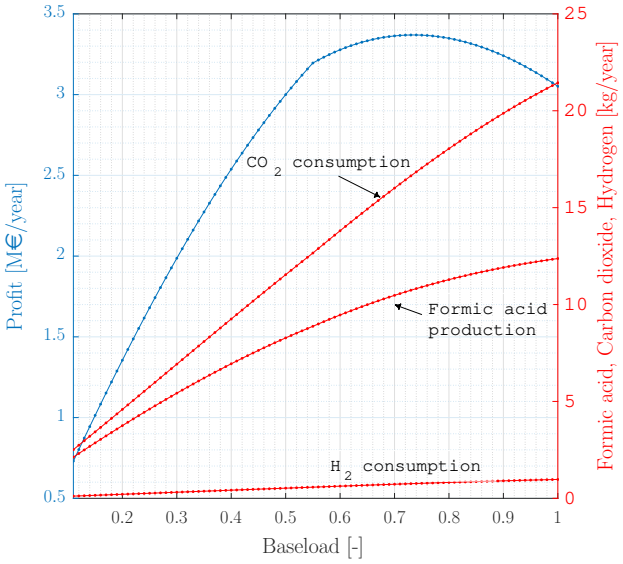


Figure 9: Profit, carbon dioxide and hydrogen consumption and formic acid production at different baseloads.

Taking into account the importance of FCR and electricity price, the sensitivity analysis is carried out to determine how variations in market prices can alter the profit. Fig. 10(a) depicts the sensitivity of the profit to FCR price, considering a fixed electricity price of 62.2 €/MWh. Fig. 10(b) shows the sensitivity analysis of profit for a range of electricity prices with a fixed FCR price of 19.6 €/MW/h. The profit variation represents the profit improvement in percentage comparing to the full-load operation. Firstly, the figures show how the profit rises with increasing electricity or FCR prices. Secondly, as either one of these prices goes up, it is worthwhile to offer more primary reserve, consequently lowering the baseload.

## 5. Dynamic simulation

After having discussed the optimal economic approach and indicating the optimal range of baseload power and power reserve, the dynamic performance of the process is investigated in this section. The power consumption of the PEM electrolyser is regulated to provide FCR by the primary control loop (section 3.1). As illustrated in Fig. 10, the optimal baseload can vary based on FCR and electricity price. Therefore, the PEM electrolyser operates at a baseload of 70% (4.05 MW), approximately the mean value of the obtained optimal range, while providing the remaining 30% of its capacity (1.74 MW) as power reserve. Fig. 12 shows the flexible operation of the electrolyser providing symmetrical 200 mHz FCR. A real 800 s grid frequency dataset is used from the synchronous grid of continental Europe, which includes the significant grid

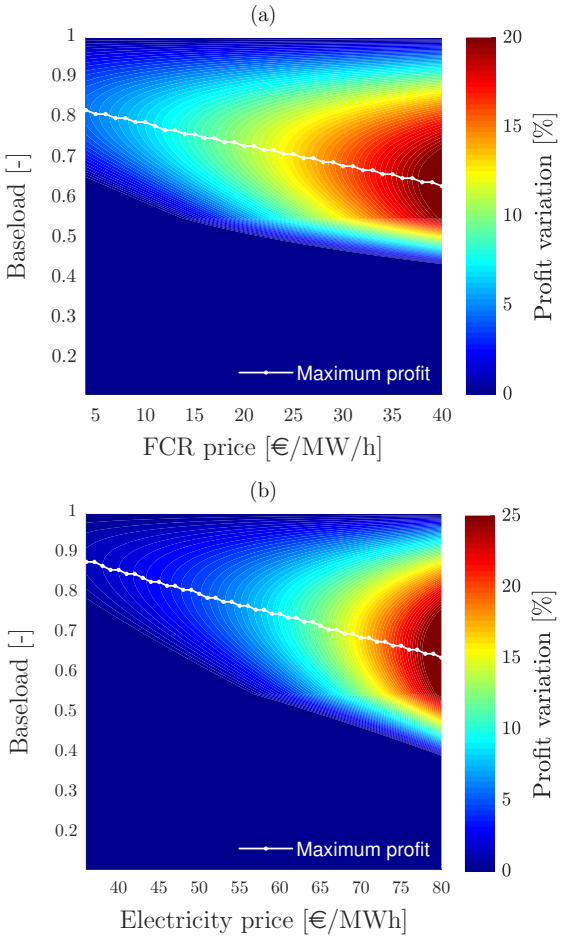


Figure 10: Sensitivity of profit to (a) FCR price and (b) electricity price.

frequency variation [47]. The frequency profile is selected to include frequency variations above and below the nominal frequency (50 Hz), allowing to monitor process dynamics for both upward and downward regulations. As illustrated in Fig. 11, the frequency profile represents an accurate estimation of the grid frequency behaviour in one year, respecting the 98% confidence interval of the frequency distribution. The data have a sampling period of 10 s, and the electrolyser responds to the grid frequency variation. The power input is regulated using a cascaded control system by controlling the PEM stack current. The electrolyser operates at the baseload when the grid frequency is within the deadband (50 Hz±10 mHz). The reference signal is the electrolyser operating setpoint $P_e$, which is the sum of baseload and power reserve calculated by $P_e = P_b + \delta P$, where activated power reserve is defined by $\delta P = k\,\delta f$. Therefore, the primary controller reacts proportionally to the grid frequency variations by regulating the electrolyser power. As illustrated in Fig. 12, when the grid frequency drops below 49.99 Hz, the electrolyser operates below the baseload. Contrarily, the electrolyser's power consumption increases above the baseload while the frequency is above 50.01 Hz. Consequently, the generated hydrogen varies based on the grid frequency variation as a result of FCR provision. As shown, the PEM dynamics are considerably fast, and it can

track the reference signal in less than five seconds. Therefore, the PEM electrolysis can be run at different power levels with a high degree of reactivity and is able to provide FCR adequately.

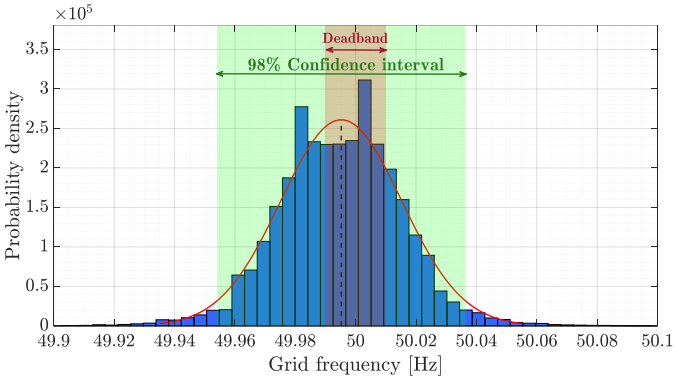


Figure 11: Grid frequency distribution in one year.

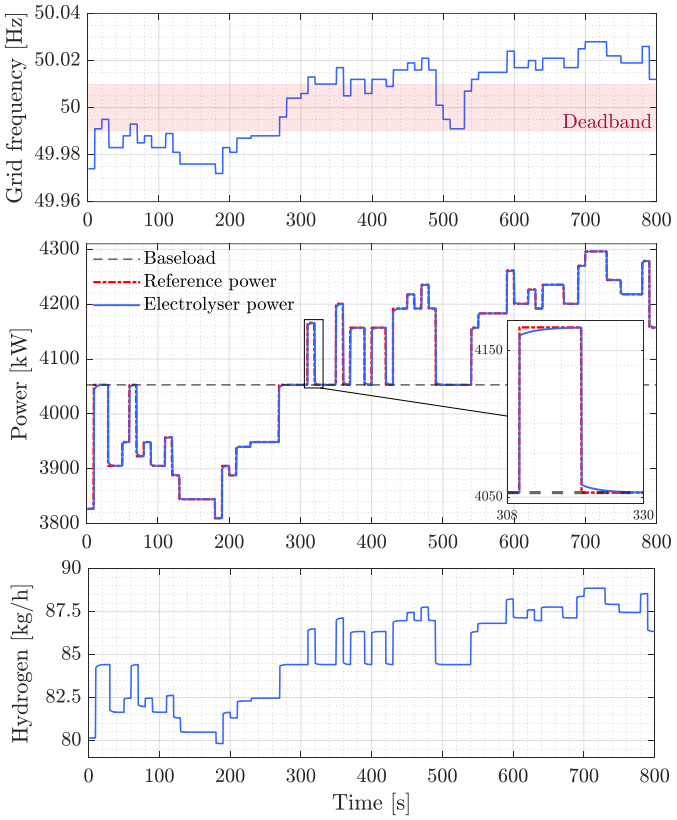


Figure 12: The dynamic performance of the PEM electrolyser under FCR provision strategy.

Fig. 13 illustrates the first compressor performance in the $H_2$ feed stream. As a result of primary level control, the hydrogen production fluctuates based on the grid frequency variation. Therefore, the first compressor in the compression stage is controlled to deliver a constant discharge pressure at different $H_2$ flow rates. As shown, the cascaded controller tracks the hydrogen variation by regulating the compressor speed. The variable compressor speed is obtained by regulating the motor torque. As shown, the discharge pressure and temperature are adequately regulated around their desired levels with minimal deviations.

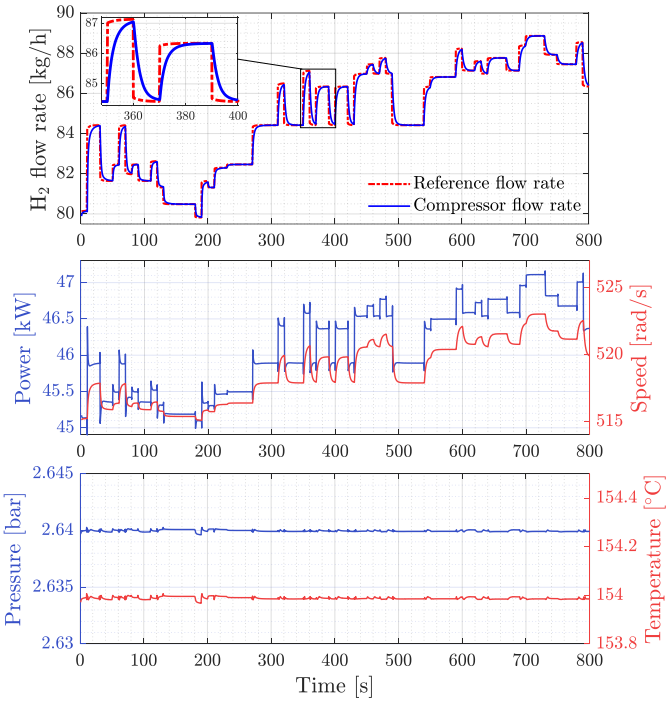


Figure 13: The dynamic performance of the first compressor in the $H_2$ compression stage.

The following four compressors in the compression stage are controlled to adjust their rotational speed based on the first compressor discharge flow rate. Fig. 14 illustrates the fifth compressor performance representing the last four compressors in the compression stage with the pressure and temperature of $H_2$ at the reactor inlet. The control diagram of the compressors is shown in Fig. 8. The reference speed signal is generated based on the $H_2$ flow rate using a lookup table obtained from the compressor performance map. As illustrated in Fig. 14, the motor speed, and consequently the power, are regulated to produce the desired pressure. As can be seen, the proposed control strategy can maintain the pressure and the temperature of $H_2$ at the optimal values.

Fig. 15 shows the dynamic performance of the first compressor in the $CO_2$ compression stage. The first compressor in the $CO_2$ stream is responsible for modifying the $CO_2$ flow rate such that the required $^{CO_2}/_{H_2}$ ratio is maintained at the reactor while supplying the desired discharge pressure. The compressor speed is regulated to adjust the $CO_2$ flow rate based on flow rate variation in the $H_2$ stream. As illustrated, the $CO_2$ and $H_2$ flow rate ratio is maintained at the desired level despite the variation in hydrogen production while the discharge pressure is maintained at a nearly constant level. In Fig. 16, the corresponding compressor performance for the 800 s simulation is illustrated on the efficiency map. As shown, for around 10% flow rate variation, the compressor operates at its maximum efficiency while the pressure ratio is maintained

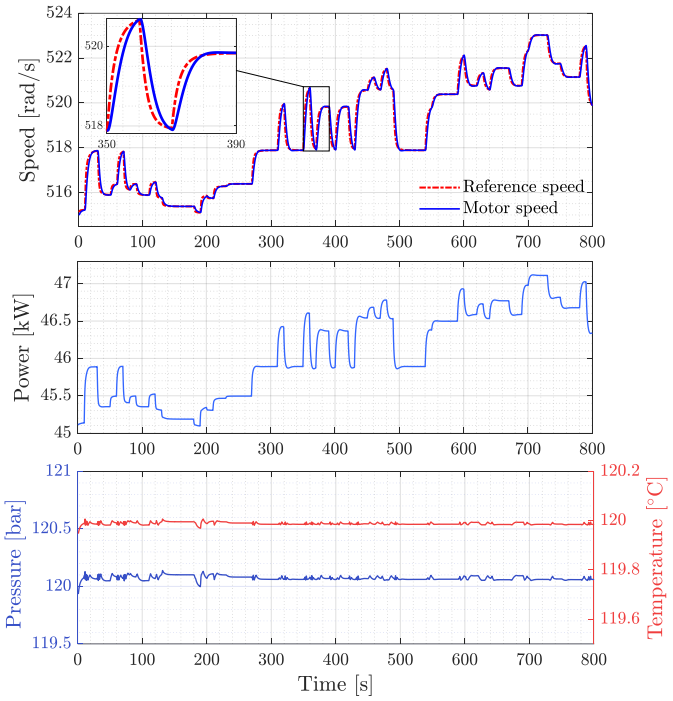


Figure 14: The dynamic performance of the fifth compressor in the $H_2$ compression stage and reactor inlet pressure and temperature.

at the desired value.

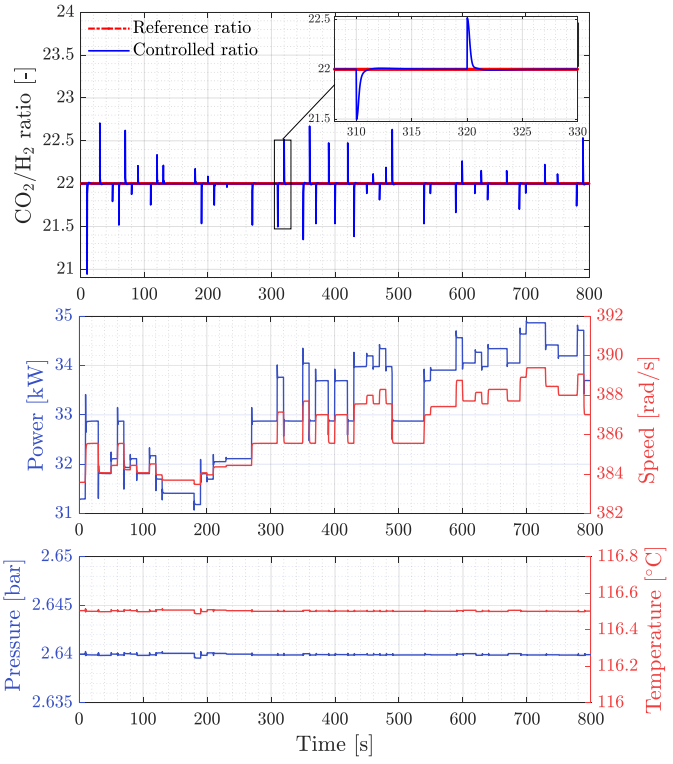


Figure 15: The dynamic performance of the first compressor in the $CO_2$ compression stage.

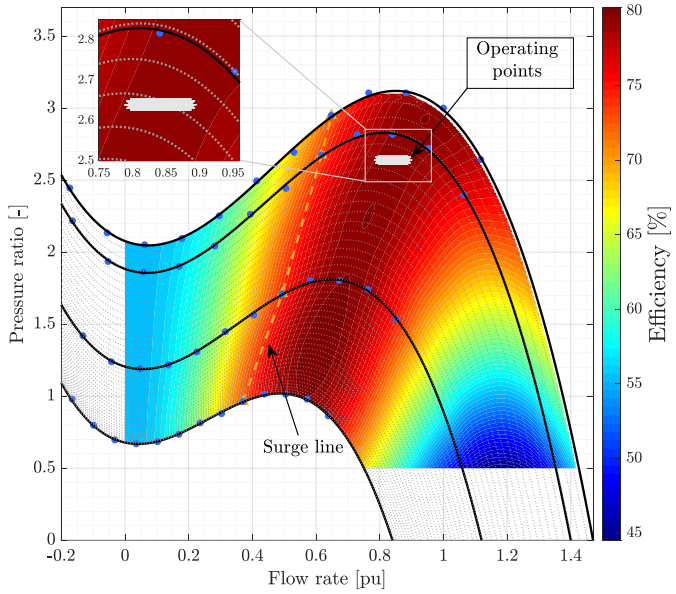


Figure 16: The performance of the first compressor in the $CO_2$ compression stage on the efficiency map.

Similar to the $H_2$ compression stage, the next four compressor speeds are regulated based on the first compressor discharge flow rate to keep the output pressures at the desired level. Fig. 17 illustrates the fifth compressor performance representing the last four compressors in the $CO_2$ compression stage. As the result of variable speed operation, the pressure and temperature of the $CO_2$ are maintained at the reactor's optimal operating condition.

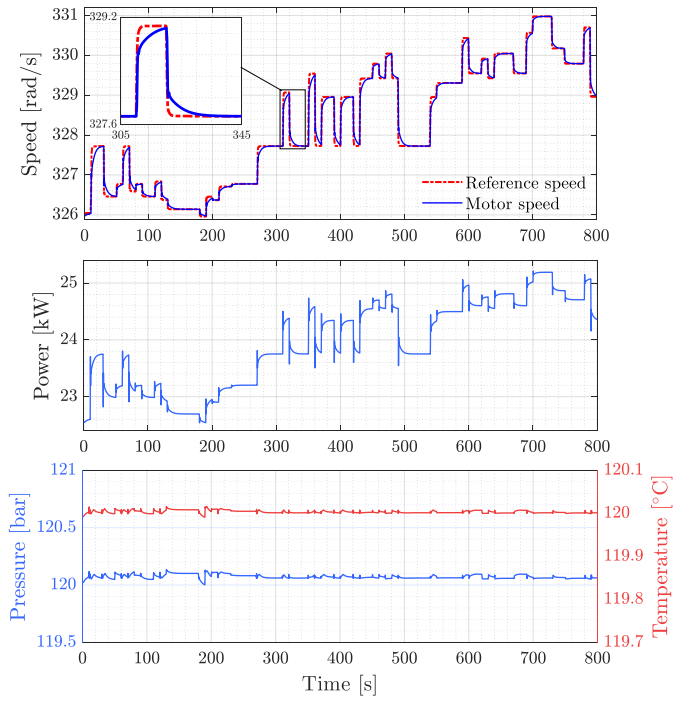


Figure 17: The dynamic performance of the fifth compressor in the $CO_2$ compression stage and reactor inlet pressure and temperature.

The simulations have been carried out for different frequency profiles to evaluate the control performance. The Root Mean Square (RMS), mean and Standard Deviation (SD) of the error are calculated for the controlled variables and the reactor operating parameters. As given in Table 2, the control system has a robust performance with limited errors in different operating conditions.

Table 2: Error statistics for controlled variables.

| | Control system | RMS | Mean | SD |
|---|---|---|---|---|
| $H_2$ stream | Electrolyser Power (kW) | 1.4572 | -0.0114 | 1.4571 |
| | Compressor 1 Flow rate (kg/h) | 0.3532 | -0.0027 | 0.3532 |
| | Compressor 5 Rotational speed (rad/s) | 0.2031 | -0.0015 | 0.2031 |
| | Reactor Inlet pressure (bar) | 0.1178 | 0.1171 | 0.0127 |
| | Reactor Inlet temperature (°C) | 0.0871 | 0.0870 | 0.0034 |
| $CO_2$ stream | Compressor 1 Flow rate ratio ($CO_2/H_2$) | 0.0351 | 0.0001 | 0.0351 |
| | Compressor 5 Rotational speed (rad/s) | 0.0931 | -0.0011 | 0.0931 |
| | Reactor Inlet pressure (bar) | 0.1180 | 0.1173 | 0.0128 |
| | Reactor Inlet temperature (°C) | 0.0033 | 0.0024 | 0.0023 |

Since the pressure and temperature are optimally controlled, the reactor product can only be influenced by the variations in the hydrogen flow rate. Fig. 18 illustrates the reactor performance under FCR provision. The AAR, productivity, and $CO_2$ conversion behave as a function of hydrogen flow rate. As the grid frequency rises, the hydrogen flow rate and productivity increases as well. Consequently, the AAR and $CO_2$ conversion rate decrease. This is to be expected since the flow rate increases reducing the residence time. As observed, for the system studied [31], 10% changes in the $H_2$ flow have a small effect in the $CO_2$ conversion rate (<1%), and even smaller changes in the AAR (<0.02%). Such variations must be considered by the separation process and are expected to have no effect in the overall efficiency of the separation [48, 49]. However, they need to be accounted for in the equipment sizing.

## 6. Discussion and Conclusions

Chemical plants with intensive electricity consumption can be engaged in grid balancing programs by providing a megawatt-scale power reserve. However, providing grid requirements is challenging due to the chemical process constraints. The chemical processes should operate flexibly to allow active participation of the chemical plant in the ancillary market. The flexible operating strategy must satisfy the grid requirements while respecting the process efficiency and constraints. Therefore, dynamic plant models and control

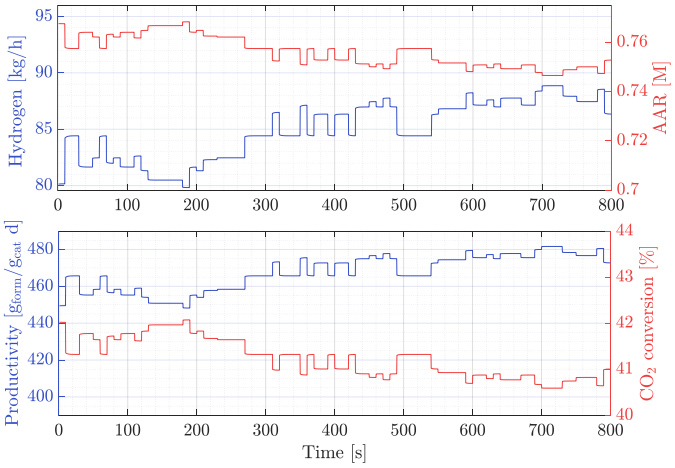


Figure 18: Reactor performance under FCR provision.

algorithms are needed to achieve the optimal flexible operation of a chemical process. In this article, a flexible operating strategy is proposed to facilitate the integration of an energy-intensive CCU based process into the power grid. The flexible operation is realised through a cooperative operation of the PEM electrolyser and the multi-stage compression systems in the process. The chemical process uses $CO_2$ and $H_2$ as raw materials to produce formic acid, which is a valuable multi-purpose chemical compound. The process is based on the continuous hydrogenation of $CO_2$ over heterogenised ruthenium catalysis. Dynamic models representing the flexible and energy-intensive process stages have been employed to investigate the FCR provision by an industrial-scale plant. The dynamic model of the process consists of a PEM electrolyser, compression stages and a reactor developed for formic acid synthesis. A control algorithm has been designed to enhance the flexibility of the process for FCR provision. The implemented control system regulates the dynamics of the process components, i.e., electrolyser and compressors, to provide ancillary services concerning process efficiency and constraints. The control system reacts to the grid frequency variations by regulating the electrolyser's power input at the primary control level. At the same time, the compressors' capacity is controlled to maintain the optimal operating condition, i.e., $CO_2$ and $H_2$ ratio, pressure and temperature. The techno-economic performance of a flexible operating strategy is assessed, and the optimal operating baseload is determined. As a result, the following conclusions can be drawn:

- Offering FCR is a valid option to create additional revenue from ancillary services.
- The optimal economic strategy is to run the electrolyser at a baseload of 73% while providing the remaining capacity as a power reserve.
- Although the formic acid production is decreased by 13%, the overall economic performance is increased by 10% by operating the process at the optimal baseload.

- Optimal operating parameters, i.e., ratio, pressure and temperature, are maintained at the reaction stage.
- FCR can be provided with a limited impact on the reaction efficiency (<1%).
- The control algorithm is robust for different operational conditions and grid frequency variations.
- The offered control strategy does not violate the reactor pressure limits.

This paper provides incentive information that can encourage more chemical plants to actively participate in the ancillary market and support the grid. Note that the proposed strategy in this paper is applicable to a variety of chemical processes in which electrolysis and compression are present, e.g., processes for direct conversion of $CO_2$ and hydrogen to value-added chemicals such as formic acid, methane and methanol. Moreover, since the proposed strategy enables the chemical process to provide FCR as the most time-critical frequency regulation product, the strategy can be efficiently applied to provide ancillary services that require a longer response time, e.g., aFRR and mFRR.

Although the proposed operating strategy enables the FCR provision and improves the process's financial revenue, a number of economic and technical considerations should be taken into account for implementation and future research and development. According to the current TSO regulations, the minimum power reserve of 1 MW is required for FCR provision, which sets a lower boundary on the process size. Therefore, smaller chemical processes with FCR reserves less than 1 MW are not allowed to participate in the ancillary market. In this work, the compressors' capacity and operating points are determined for the proposed flexible operation, while existing compression stages in chemical processes are already designed based on the process requirement without considering the FCR provision. Therefore, the available power reserve might be limited by the capacity of the compressors, and an upgrade might be required for the optimal operation, e.g., adding compression stages or adapting the compressors. Thus, the most effective approach for optimal contribution in the ancillary market is to consider the proposed demand response operation during the planning phase rather than later in the upgrading phase, which guarantees technical and economic feasibility. Moreover, the optimal baseload and power reserve might be influenced by the uncertain behaviour of the energy and reserve markets. Therefore, applying stochastic optimisation and prediction techniques in future work can improve the bidding strategy to deal with the uncertainties in the market price and support optimal operating decisions. Furthermore, the operational flexibility offered by the proposed strategy facilitates the cooperative operation of the chemical plant with renewable energy sources, where the chemical process can operate as a buffer, utilising the excess generated power for upward and downward regulation services.

## 7. Acknowledgments

This work was performed in the framework of the Catalisti cluster SBO project CO2PERATE ("All renewable CCU based on formic acid integrated in an industrial microgrid"), with the financial support of VLAIO (Flemish Agency for Innovation and Entrepreneurship). César A. Urbina-Blanco acknowledges financial support from a senior postdoctoral fellowship from the Fund for Scientific Research Flanders (FWO).

## References

[1] Communication from the Commission to the European Parliament, the Council, the European Economic and Social Committee and the Committee of the Regions. A policy framework for climate and energy in the period from 2020 up to 2030 (2014), URL: https://eur-lex.europa.eu/legal-content/EN/ALL/?uri=celex%3A52014DC0015.

[2] S. D. Ahmed, F. S. Al-Ismail, M. Shafiullah, F. A. Al-Sulaiman, I. M. El-Amin, Grid integration challenges of wind energy: A review, IEEE Access 8 (2020) 10857–10878, DOI: 10.1109/ACCESS.2020.2964896.

[3] N. Mansouri, A. Lashab, J. M. Guerrero, A. Cherif, Photovoltaic power plants in electrical distribution networks: a review on their impact and solutions, IET Renewable Power Generation 14 (12) (2020) 2114–2125, DOI: 10.1049/iet-rpg.2019.1172.

[4] M. Musau, Security and stability aspects of multi objective dynamic economic dispatch with renewable energy and HVDC transmission lines, Journal of Power and Energy Engineering 6 (09) (2018) 165, DOI: 10.4236/jpee.2018.69013.

[5] M. Paulus, F. Borggrefe, The potential of demand-side management in energy-intensive industries for electricity markets in germany, Applied Energy 88 (2) (2011) 432–441, DOI: 10.1016/j.apenergy.2010.03.017.

[6] M. Manana, A. Zobaa, A. Vaccaro, A. Arroyo, R. Martinez, P. Castro, A. Laso, S. Bustamante, Increase of capacity in electric arc-furnace steel mill factories by means of a demand-side management strategy and ampacity techniques, International Journal of Electrical Power & Energy Systems 124 (2021) 106337, DOI: 10.1016/j.ijepes.2020.106337.

[7] L. C. Brée, K. Perrey, A. Bulan, A. Mitsos, Demand side management and operational mode switching in chlorine production, AIChE Journal 65 (7) (2019) e16352, DOI: 10.1002/aic.16352.

[8] B. Bruns, A. Di Pretoro, M. Grünewald, J. Riese, Flexibility analysis for demand-side management in large-scale chemical processes: An ethylene oxide production case study, Chemical Engineering Science 243 (2021) 116779, DOI: 10.1016/j.ces.2021.116779.

[9] C. Tsay, A. Kumar, J. Flores-Cerrillo, M. Baldea, Optimal demand response scheduling of an industrial air separation unit using data-driven dynamic models, Computers & Chemical Engineering 126 (2019) 22–34, DOI: 10.1016/j.compchemeng.2019.03.022.

[10] A. Caspari, C. Tsay, A. Mhamdi, M. Baldea, A. Mitsos, The integration of scheduling and control: Top-down vs. bottom-up, Journal of Process Control 91 (2020) 50–62, DOI: 10.1016/j.jprocont.2020.05.008.

[11] D. L. Summerbell, D. Khripko, C. Barlow, J. Hesselbach, Cost and carbon reductions from industrial demand-side management: Study of potential savings at a cement plant, Applied energy 197 (2017) 100–113, DOI: 10.1016/j.apenergy.2017.03.083.

[12] X. Xu, M. Abeysekera, C. Gutschi, M. Qadrdan, K. Rittmannsberger, W. Markus, J. Wu, N. Jenkins, Quantifying flexibility of industrial steam systems for ancillary services: a case study of an integrated pulp and paper mill, IET Energy Systems Integration 2 (2) (2020) 124–132, DOI: 10.1049/iet-esi.2019.0082.

[13] K. Seo, T. F. Edgar, M. Baldea, Optimal demand response operation of electric boosting glass furnaces, Applied Energy 269 (2020) 115077, DOI: 10.1016/j.apenergy.2020.115077.

[14] D. Fabozzi, N. F. Thornhill, B. C. Pal, Frequency restoration reserve control scheme with participation of industrial loads, in: 2013 IEEE Conference, Grenoble, France, 2013, DOI: 10.1109/PTC.2013.6652104.

[15] K. Arnold, T. Janßen, Demand side management in industry : necessary for a sustainable energy system or a backward step in terms of improving efficiency?, in: Going beyond energy efficiency to deliver savings, competitiveness and a circular economy : ECEEE

Industrial Summer Study proceedings ; 12-14 September 2016, Die Kalkscheune, Berlin, Germany, Europ. Council for an Energy Efficient Economy, Stockholm, 2018, pp. 339 – 350, URL: https://nbn-resolving.org/urn:nbn:de:bsz:wup4-opus-69405.

[16] M. Cheng, J. Wu, S. J. Galsworthy, C. E. Ugalde-Loo, N. Gargov, W. W. Hung, N. Jenkins, Power system frequency response from the control of bitumen tanks, IEEE Transactions on Power Systems 31 (3) (2015) 1769–1778, DOI: 10.1109/TPWRS.2015.2440336.

[17] X. Zhang, G. Hug, J. Z. Kolter, I. Harjunkoski, Demand response of ancillary service from industrial loads coordinated with energy storage, IEEE Transactions on Power Systems 33 (1) (2017) 951–961, DOI: 10.1109/TPWRS.2017.2704524.

[18] J. I. Otashu, M. Baldea, Scheduling chemical processes for frequency regulation, Applied Energy 260 (2020) 114125, DOI: 10.1016/j.apenergy.2019.114125.

[19] F. Klaucke, C. Hoffmann, M. Hofmann, G. Tsatsaronis, Impact of the chlorine value chain on the demand response potential of the chloralkali process, Applied Energy 276 (2020) 115366, DOI: 10.1016/j.apenergy.2020.115366.

[20] D. Todd, M. Caufield, B. Helms, A. P. Generating, I. M. Starke, B. Kirby, J. Kueck, Providing reliability services through demand response: A preliminary evaluation of the demand response capabilities of alcoa inc, ORNL/TM 233, DOI: 10.2172/948544 (2008).

[21] A. E. Samani, A. D'Amicis, J. D. M. De Kooning, D. Bozalakov, P. Silva, L. Vandevelde, Grid balancing with a large-scale electrolyser providing primary reserve, IET Renewable Power Generation 14 (16) (2020) 3070–3078, DOI: 10.1049/iet-rpg.2020.0453.

[22] A. Dadkhah, D. Bozalakov, J. D. M. De Kooning, L. Vandevelde, On the optimal planning of a hydrogen refuelling station participating in the electricity and balancing markets, International Journal of Hydrogen Energy 46 (2) (2021) 1488–1500, DOI: 10.1016/j.ijhydene.2020.10.130.

[23] L. Allidières, A. Brisse, P. Millet, S. Valentin, M. Zeller, On the ability of PEM water electrolysers to provide power grid services, International Journal of Hydrogen Energy 44 (20) (2019) 9690–9700, DOI: 10.1016/j.ijhydene.2018.11.186.

[24] M. Pérez-Fortes, E. Tzimas, et al., Techno-economic and environmental evaluation of $CO_2$ utilisation for fuel production, Synthesis of methanol and formic acid, 2016, DOI: 10.2790/89238.

[25] A. Álvarez, A. Bansode, A. Urakawa, A. V. Bavykina, T. A. Wezendonk, M. Makkee, J. Gascon, F. Kapteijn, Challenges in the greener production of formates/formic acid, methanol, and DME by heterogeneously catalyzed $CO_2$hydrogenation processes, Chemical reviews 117 (14) (2017) 9804–9838, DOI: 10.1021/acs.chemrev.6b00816.

[26] D. Mellmann, P. Sponholz, H. Junge, M. Beller, Formic acid as a hydrogen storage material–development of homogeneous catalysts for selective hydrogen release, Chemical Society Reviews 45 (14) (2016) 3954–3988, DOI: 10.1039/C5CS00618J.

[27] J. Artz, T. E. Müller, K. Thenert, J. Kleinekorte, R. Meys, A. Sternberg, A. Bardow, W. Leitner, Sustainable conversion of carbon dioxide: an integrated review of catalysis and life cycle assessment, Chemical reviews 118 (2) (2018) 434–504, DOI: 10.1021/acs.chemrev.7b00435.

[28] Marketsandmarkets. formic acid market by types, application & geography, 2019, URL: https://www.marketsandmarkets.com/Market-Reports/formic-acid-Market-69868960.html.

[29] Oec. formic acid product trade, exporters and importers, the observatory of economic complexity, URL: https://oec.world/en/profile/hs92/formic-acid?redirect=true.

[30] Z. Ma, U. Legrand, E. Pahija, J. R. Tavares, D. C. Boffito, From $co_2$ to formic acid fuel cells, Industrial & Engineering Chemistry Research 60 (2) (2020) 803–815, DOI: 10.1021/acs.iecr.0c04711.

[31] K. Park, G. H. Gunasekar, S.-H. Kim, H. Park, S. Kim, K. Park, K.-D. Jung, S. Yoon, $CO_2$ hydrogenation to formic acid over heterogenized ruthenium catalysts using a fixed bed reactor with separation units, Green Chemistry 22 (5) (2020) 1639–1649, DOI: 10.1039/C9GC03685G.

[32] Q. Wang, S. Santos, C. A. Urbina-Blanco, W. Y. Hernández, M. Impéror-Clerc, E. I. Vovk, M. Marinova, O. Ersen, W. Baaziz, O. V. Safonova, et al., Solid micellar Ru single-atom catalysts for the water-free hydrogenation of $CO_2$ to formic acid, Applied Catalysis B: Environmental 290 (2021) 120036, DOI: 10.1016/j.apcatb.2021.120036.

[33] Y. Matsubara, D. C. Grills, Y. Koide, Thermodynamic cycles relevant to hydrogenation of $CO_2$ to formic acid in water and acetonitrile, Chemistry Letters 48 (7) (2019) 627–629, DOI: 10.1246/cl.190180.

[34] J. J. Anderson, D. J. Drury, J. E. Hamlin, A. G. Kent, Process for the preparation of formic acid (WO1986002066A1), 2019, URL: https://patentscope.wipo.int/search/en/detail.jsf?docId=WO1986002066.

[35] M. Mohanpurkar, Y. Luo, D. Terlip, F. Dias, K. Harrison, J. Eichman, R. Hovsapian, J. Kurtz, Electrolyzers enhancing flexibility in electric grids, Energies 10 (11) (2017) 1836, DOI: 10.3390/en10111836.

[36] B. W. Tuinema, E. Adabi, P. K. Ayivor, V. G. Suárez, L. Liu, A. Perilla, Z. Ahmad, J. L. R. Torres, M. A. van der Meijden, P. Palensky, Modelling of large-sized electrolysers for real-time simulation and study of the possibility of frequency support by electrolysers, IET Generation, Transmission & Distribution 14 (10) (2020) 1985–1992, DOI: 10.1049/iet-gtd.2019.1364.

[37] R. F. Mann, J. C. Amphlett, M. A. Hooper, H. M. Jensen, B. A. Peppley, P. R. Roberge, Development and application of a generalised steady-state electrochemical model for a PEM fuel cell, Journal of power sources 86 (1-2) (2000) 173–180, DOI: 10.1016/S0378-7753(99)00484-X.

[38] M. Rubio, A. Urquia, S. Dormido, Diagnosis of PEM fuel cells through current interruption, Journal of Power Sources 171 (2) (2007) 670–677, DOI: 10.1016/j.jpowsour.2007.06.072.

[39] C. Martinson, G. Van Schoor, K. Uren, D. Bessarabov, Equivalent electrical circuit modelling of a proton exchange membrane electrolyser based on current interruption, in: 2013 IEEE International Conference on Industrial Technology (ICIT), IEEE, 2013, pp. 716–721, DOI: 10.1109/ICIT.2013.6505760.

[40] K. Darowicki, L. Gawel, Impedance measurement and selection of electrochemical equivalent circuit of a working PEM fuel cell cathode, Electrocatalysis 8 (3) (2017) 235–244, DOI: 10.1007/s12678-017-0363-0.

[41] C. A. Martinson, G. Van Schoor, K. Uren, D. Bessarabov, Characterisation of a PEM electrolyser using the current interrupt method, International journal of hydrogen energy 39 (36) (2014) 20865–20878, DOI: 10.1016/j.ijhydene.2014.09.153.

[42] J. D. M. De Kooning, J. Van de Vyver, B. Meersman, L. Vandevelde, Maximum efficiency current waveforms for a PMSM including iron losses and armature reaction, IEEE Transactions on Industry Applications 53 (4) (2017) 3336–3344, DOI: 10.1109/TIA.2017.2681619.

[43] B.-H. Bae, S.-K. Sul, J.-H. Kwon, J.-S. Byeon, Implementation of sensorless vector control for super-high-speed PMSM of turbo-compressor, IEEE Transactions on Industry Applications 39 (3) (2003) 811–818, DOI: 10.1109/TIA.2003.810658.

[44] FCR service design note, April 2019, URL: https://www.elia.be/-/media/project/elia/elia-site/electricity-market-and-system—document-library/balancing—balancing-services-and-bsp/2019/2019-design-note-fcr-for-2020.pdf.

[45] Establishing a guideline on electricity transmission system operation, Official Journal of the European UnionURL: https://eur-lex.europa.eu/ (2017).

[46] M. Pérez-Fortes, J. C. Schöneberger, A. Boulamanti, G. Harrison, E. Tzimas, Formic acid synthesis using $CO_2$ as raw material: Techno-economic and environmental evaluation and market potential, International Journal of Hydrogen Energy, volume=41, number=37, pages=16444–16462, year=2016, publisher=Elsevier, note=DOI: 10.1016/j.ijhydene.2016.05.199.

[47] Frequency and fcr demand per 10 secondsURL: https://opendata.elia.be/explore/dataset/ods057/information/.

[48] K. Narita, M. Sekiya, Vapor-liquid equilibrium for formic acid-triethylamine system examined by the use of a modified still. formic acid-trialkylamine azeotropes, Chemical and Pharmaceutical Bulletin 25 (1) (1977) 135–140, DOI: 10.1248/cpb.25.135.

[49] J. Hietala, A. Vuori, P. Johnsson, I. Pollari, W. Reutemann, H. Kieczka, Formic acid, Ullmann's encyclopedia of industrial chemistry 1 (2016) 1–22, DOI: 10.1002/14356007.a12_013.pub3.